A comparison of X-ray and NMR structures for human endothelin-1

B.A. WALLACE,[1] ROBERT W. JANES,[1] DONNA A. BASSOLINO,[2] AND
STANLEY R. KRYSTEK, JR.[2]

[1] Department of Crystallography, Birkbeck College, University of London, London WC1E 7HX, United Kingdom
[2] Department of Macromolecular Modeling, Bristol-Myers Squibb Pharmaceutical Research Institute,
  Princeton, New Jersey 08543

Abstract

Direct comparisons between the recently solved X-ray and NMR structures of human endothelin-1 with respect
to secondary structure, RMS deviations, surface accessibilities, and side-chain conformers indicate important dif-
ferences in conformation, especially in the C-terminus, but also in the central loop region, that are important for
defining the specificity of binding. These differences are larger than seen for other X-ray and NMR structures
that have been compared. Comparisons between the X-ray structure and the NMR NOE constraints highlight the
regions of flexibility and environment-induced diversity in the endothelin structures.

Keywords: drug design; endothelin; NMR spectroscopy; vasoconstrictor; X-ray crystallography

For macromolecules of medical importance, especially those that
are targets for rational drug design, it is crucial to have details
of their three-dimensional structures. Traditionally this informa-
tion has been provided by single crystal X-ray analysis. However,
recent technical advances have meant that NMR spectroscopy
has proven to be a valuable alternative to crystallography, es-
pecially for polypeptides of intermediate size, where NMR mea-
surements are relatively facile and X-ray phase determination
is particularly difficult. The major problem for NMR occurs
when the molecule is small and very flexible or has an unordered
conformation. However, if the molecule has conformational re-
strictions such as disulfide bridges that produce a globular struc-
ture, this enables the use of NMR spectroscopic techniques.
Endothelin (ET), a 21-amino acid polypeptide with disulfide
links between residues 1 and 15, and 3 and 11, respectively, is
a molecule that has proven to be a popular target for NMR stud-
ies (Table 1) because its crosslinks provide considerable con-
straints in the N-terminus of the molecule. ET is also one of the
few molecules in this size range whose structure has been solved
by crystallographic methods (Janes et al., 1994) and hence pro-
vides an important opportunity for comparisons of the solution
and solid state structures.

Previously, independent X-ray and NMR studies have been
done on the same molecule and the resulting structures com-
pared (Billeter et al., 1989), or X-ray structures have preceded

the NMR structures and either aided in their interpretation or
were used as a criterion for acceptability of the NMR models
(Brünger et al., 1986), or structures have been jointly refined
using both NMR and X-ray constraints (Shaanan et al., 1992).
In an early study, Brünger et al. (1987) used crambin as a test
system for employing an NMR structure for molecular replace-
ment. But, to our knowledge, the only success in a de novo de-
termination of an X-ray structure using an intact NMR model
for molecular replacement phasing of the X-ray data (Baldwin
et al., 1991) was achieved using the NMR structure of interleukin-8
(IL-8). This was a case where the X-ray and NMR structures
closely corresponded. ET represents the first instance of the suc-
cessful use of a *partial* NMR-derived model for phasing the
X-ray data of a polypeptide structure. In this case, the many
NMR models for the structure (Table 1) showed significant con-
formational variance with each other and, ultimately, with the
X-ray structure, to the extent that, of the many models tried
(Krystek et al., 1991; Andersen et al., 1992), only one was close
enough to produce a molecular replacement solution (Krystek
et al., 1991) and that only when nearly 40% of the molecule had
been removed. All the complete NMR models tested were un-
successful in molecular replacement, suggesting that they were
very different from the X-ray structure. Only when a fragment
consisting of the 16 N-terminal residues was used did one NMR
model produce a successful molecular replacement solution.
Therefore, comparison of that ET NMR model and the X-ray
structure may be particularly interesting because of the larger
divergences between the structures than in the previous
examples.

Table 1. *Reported conformations of endothelin-1 determined by NMR*[a]

N-terminus	Turn	Helix	C-terminus	Solvent	Author
1-4 (A)	5-8	9-16	Extended	60% ethylene glycol/H_2O with TFA	Krystek et al. (1991)
Extended 1-4	N	9-15	N	DMSO	Endo et al. (1989)
N	N	6-11	N	DMSO	Munro et al. (1991)
N	N	N	Associated with core	DMSO	Saudek et al. (1989)
N	N	9-15	Associated with core	DMSO with TFA	Saudek et al. (1991)
1-4 (A)	5-8 (A)	9-15	A	60% ethylene glycol/H_2O with TFA	Andersen et al. (1992)
Extended 1-4	5-8	9-15	N	10% acetic acid/H_2O	Tamaoki et al. (1991)
N	N	9-15	A	30% CD_3CN/H_2O	Reily and Dunbar (1991)
Extended	N	9-16	A	50% CD_3CN/H_2O	Aumelas et al. (1991)
Extended	5-8	9-16	Extended	40% acetic acid/H_2O	Dalgarno et al. (1992)
N	5-8	9-15	A	10% CH_3CN, 1.5% acetic acid/H_2O	Coles et al. (1994)

[a] A, evidence of conformational averaging; N, no preferred conformation could be identified; TFA, trifluoroacetic acid.

In this paper, we will focus on comparisons between the closest NMR model, that is, the one that was successful in producing the molecular replacement solution, and the ultimate X-ray crystal structure. However, we will also examine some of the differences found for the other NMR models that were not sufficiently close in structure to produce a molecular replacement solution, in order to see how they deviate from the canonical structure.

Results

Comparisons between the X-ray and NMR structures

The ET X-ray structure has been described as having an N-terminal extended β-strand with a bulge between residues 5 and 7, a hydrogen bonded loop between the carbonyl oxygen of residue 7 and the amide proton of residue 11, followed by a long, somewhat irregular helix extending from residue 9 to the C-terminus (Fig. 1A). The NMR structure could be described as having a conformationally averaged N-terminus between residues 1 and 4, which are in a β-strand structure with residues 5-8 forming a turn, and residues 9-16 being helical. Its C-terminus is extended and flexible (Fig. 1B). Thus, the two structures do have common features but also differ significantly in detail. The most notable difference, of course, is the nature of the six C-terminal residues (Figs. 1, 2).

The regions around the disulfide bonds of the two structures are very comparable, as is the helical region between the cysteines at residues 11 and 15, and to a lesser extent, the backbone of the region between the cysteines at residues 1 and 3 (all color-coded blue in Fig. 2). However, the central loop/turn, especially residue 9 and the side chains of residues 5 and 6, are very different (Fig. 2) as, of course, is the C-terminal tail (color-coded red in Fig. 2).

The hydrogen bonding patterns in the "head" region (the designation for residues 1-15) are also different: In the X-ray structure, this region is stabilized by main-chain–main-chain hydrogen bonds between residues 7 and 11, and 6 and 8, respectively, whereas in the NMR model, the main-chain–main-chain hydrogen bonds are between residues 9 and 13, and 10 and 14, respectively. Both structures have a hydrogen bond between residues 11 and 15.

The ϕ and ψ angles (Fig. 3A,B) for the stretch of residues from Lys 9 to Ile 20 of the X-ray structure fall in the general helix region of the Ramachandran plot according to PROCHECK (Laskowski et al., 1993), whereas only those from residues 10 to 16 in the NMR model are what would be considered helical based on this criterion. The long helix in the X-ray structure is somewhat irregular. The helical hydrogen bonding pattern extends through residue 20 in the X-ray structure and to residue 15 in the NMR structure.

The central region of the molecule is tightly constrained by the disulfide crosslinks and hence there are more NOEs per residue involving the cysteines and the residues in the helix between Cys 11 and Cys 15 (Fig. 4A); this well-defined region corresponds most closely to the X-ray structure. However, the N- and C-termini are relatively poorly defined by the NMR structural constraints, perhaps accounting for their greater divergence from the X-ray structure.

The patterns of surface accessibilities (Lee & Richards, 1971) of the NMR and X-ray structures also differ significantly, particularly in the region around residues 5-7 and, to a lesser extent, in the tail region (Fig. 5). These differences could be important with respect to substitution of alternate amino acid types that are present in the endothelin isoforms (Janes & Wallace, 1994). Specifically, Ser 5 and Leu 6 are considerably less buried in the X-ray structure than in the NMR structure. This means that the much larger side chains found in the ET2 and ET3 isoforms (e.g., Trp instead of Leu at position 6) could more easily fit into the X-ray structure without disrupting the overall fold. Residue 2, which is Ser in ET1 or the bulkier Thr in ET3, is also more accessible in the X-ray structure. In contrast, residue 7, Met in ET1, has considerable accessibility in both structures, but somewhat less in the X-ray structure than in the NMR model; however, as the isoform substitutions at this position are Leu and Lys, which are not that much different in size, surface exposure may not be so important at this site. Thus, the exposed surface areas of the variable residues differ considerably between the two structures, whereas the extent of exposure of the conserved residues is more similar.

Another measure of side-chain conformational variation is the chi1 rotamers that are employed by the two structures (Fig. 6). The pattern of use of *gauche+*, *gauche−*, and *trans* conformations is very similar for the most part in the N-terminus, although there are some differences elsewhere. Once again, residue
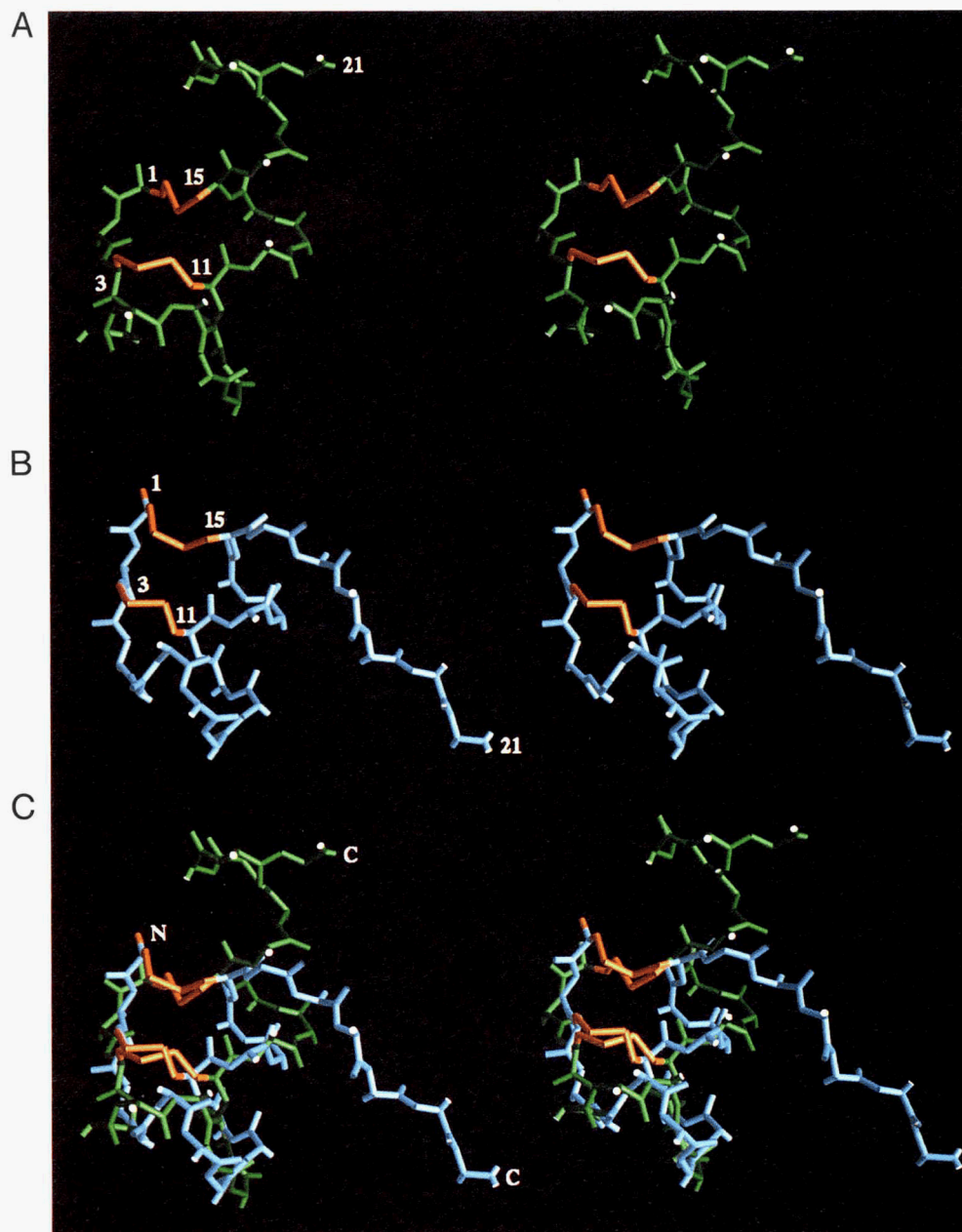
Fig. 1. Stereo views of the backbones of the (**A**) X-ray and (**B**) NMR structures, separately, and (**C**) shown overlaid.

9 is the major site of discrepancy in the head region (it is *trans* in the X-ray structure, but *gauche−* in the NMR model), whereas many of the tail residues (positions 16, 18, 20, and 21) differ in which rotamer they adopt.

Differences can also be seen in the isopotential contours around the X-ray and NMR structures (Fig. 7A,B). The distinct negative contours correspond to the charged residues and the C-terminus, which are separated by the smaller positive contours produced by the N-terminus, Lys 9, and His 16. The pattern of the contours is obviously different for the two structures. Needless to say, the electrostatic properties of this molecule are essential to receptor binding and function, so the precise nature of the conformation is essential for drug discovery efforts, and these electrostatic differences may be very significant.

Comparisons of the optimally aligned NMR and X-ray structures revealed the regions of highest similarities. Superimposing the intact structures results in an RMS difference in backbone atom positions of 4.98 Å, whereas superimposing solely residues 1–15 produces an RMS deviation of only 2.02 Å (Table 2).

What is notable from the plots (Fig. 8) of the RMS deviations of individual residues (both the backbone and side chains) is that the residues in the N-terminal region (to residue 17) are very similar, but that the deviations in positions C-terminal to that are enormous. Within the N-terminus, there are some parts that are more at variance than others, especially residues 5–9 (backbone), residues 5–9 (Cα positions), and residues 5, 6, 7, and 9 (side chains). Interestingly, these residues mostly encompass the principal variable residues in the ET isoforms.
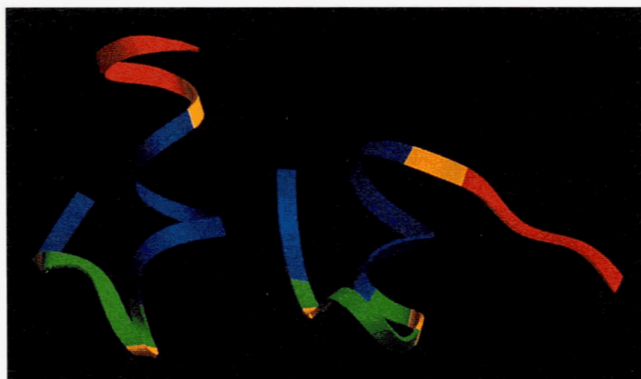
Fig. 2. Ribbon diagrams of the X-ray and NMR structures colored according to RMS deviations. Red, >10 Å; orange, 4–10 Å; green, 2–4 Å; blue, <2 Å.

The magnitudes of the deviations can be compared with those obtained for other pairs of X-ray and NMR structures. In general, close correspondences between independently determined X-ray and NMR structures (<1–2 Å RMS deviation for the backbones) have been observed for larger polypeptides (Brünger et al., 1986; Billeter et al., 1989; Smith et al., 1994). In the one other case in which an NMR model was used in the solution of the X-ray structure, IL-8 (Baldwin et al., 1991), the RMS deviation for the main-chain atoms of the intact IL-8 monomer was 1.1 Å as opposed to 3.9 Å for the intact ET structures. However, if we consider the deviation for only the head region of ET1 (2.0 Å), the deviation is more similar to that for the complete IL-8 molecule. The maximum deviation for the Cα atoms in the case of the superimposable fragment of ET is considerably

greater (>5.0 Å) than for all the Cα atoms of IL-8 (approximately 4.0 Å), suggesting that some regions of the ET X-ray and NMR models are significantly more different from each other than are the IL-8 solution and solid state structures. The larger differences between the X-ray and NMR structures for ET are likely to be, in part, a consequence of the smaller size of this polypeptide, which results in a more flexible molecule, and the significantly smaller number of long-range constraints in its NMR data, which give rise to more ambiguity in even the head region of the structure.

The dissimilarities between the X-ray and NMR structures of ET cannot be accounted for by the close contacts in the crystal. The tail is not a region where intermolecular crystal contacts occur, nor is residue 9, these being the regions of greatest divergence between the crystal and NMR structures. Indeed, the most significant van der Waals interactions in the crystal are intermolecular ones in the region between residues 12 and 15 (Janes et al., 1994), the part of the structure that is most similar in the solution and solid state models.

Also of note is that the NMR model would not actually fit into the crystal unit cell. When the NMR model is placed in the same orientation as the X-ray structure, there are dramatic clashes between adjacent symmetry-related molecules. Hence, the NMR structure would have required a cell with different dimensions to accommodate it. Furthermore, the tightest interaction in the crystal (the "dimer" contact) (Jones et al., 1994) could not form for the solution structure, as it would also produce significant van der Waals clashes.

Finally, as a general measure of stability of structures in solution, one can compare the ratio of the nonpolar to polar side-chain accessibilities in the two models. For the X-ray structure, this ratio is 1.11, whereas for the NMR structure, it is 1.35. With more buried nonpolar residues in the X-ray structure, this could potentially indicate the X-ray structure to be a slightly more stable conformation than the NMR structure.
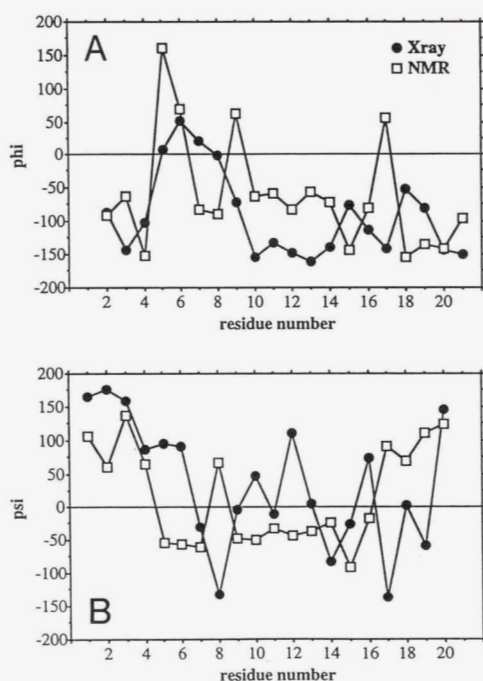
Comparisons with other NMR models

Because no unique or consensus NMR structure for ET had been produced (Table 1), different members of some of the families of structures proposed based on the NMR data (Krystek et al., 1991; Andersen et al., 1992) had been tested for use in the molecular replacement procedure. Model 1 is the successful NMR model described above, model 3 is the NMR model that was initially deposited in the PDB (Andersen et al., 1992), and models 2 and 4 are alternative models based on the same data, but calculated with different constraint algorithms (Krystek et al., 1991). None of these latter models produced a molecular replacement solution.

All of these intact models have very large RMS deviations from the X-ray structure. When only the N-terminal regions (residues 1–15) of the structures are compared, however, the correspondences are considerably better (Table 2). It is notable that the RMS deviation of the "successful" model differs from the "unsuccessful" models by only 0.3 Å, showing how finicky the procedure of molecular replacement can be.

More detailed comparisons of the four NMR models show that model 1 not only has the lowest overall RMS deviation from the X-ray structure, but also has the smallest maximum deviation from that structure (Fig. 9) in the region from residues 1 to 16. Furthermore, the disulfides of model 1 more closely su-
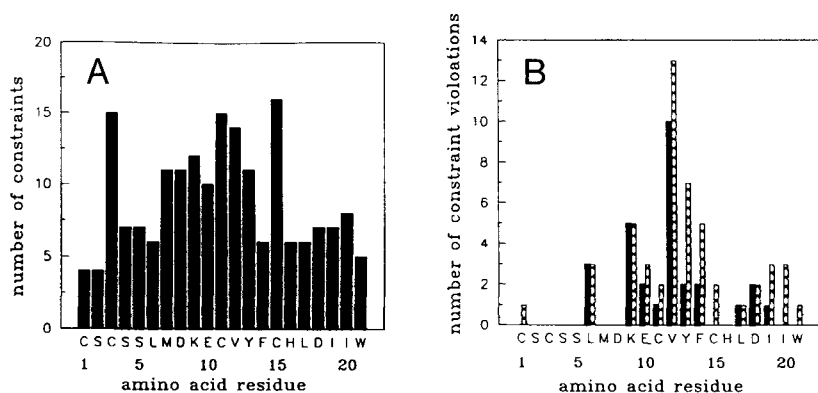

Fig. 3. Plots of **(A)** φ and **(B)** ψ angles versus residue number for the X-ray (filled circles) and NMR (open squares) structures.

Fig. 4. Histograms of (**A**) the number of NOEs versus residue number and (**B**) the number of NOE violations for the X-ray model that are greater than 2 Å (solid) or greater than 1 Å (cross hatched).

perimpose with those in the X-ray structure and thus the RMS deviation of only the sulfur atoms in the structures is also considerably smaller for model 1 (Table 2). The main chains of the other models deviate more from the X-ray model on a residue-by-residue basis in the head region, except for residues 6 and 7 of two of the models and residue 5 of one of the models. Most significantly, all the models diverge substantially from the X-ray structure starting at residue 17, a result that is in good accord with our observation that we could only use residues 1–16 for the molecular replacement.

Environmental influences on the conformation of ET

Our goal now is to try to understand the molecular nature underlying the observed differences in the X-ray and NMR structures. Even though ET is a relatively small polypeptide, with considerable conformational restraints due to its two disulfide crosslinks, the structures that have been proposed for it vary considerably, not only between the NMR and X-ray structures, but especially among the different NMR models. We need, therefore, to consider if the observed variations are due to real differences in the structures as a function of environment, are a consequence of true flexibility of the molecule, or are due to the different types of data and interpretations inherent in the different techniques.

First, we must consider the variability of the reported structures derived from NMR spectroscopy alone (Table 1). The NMR models obviously differ enormously in the conformations of their C-termini, but also vary considerably in the details of

the residues in the head region. Many of these variations are a consequence of the experimental conditions. Because of the lack of solubility of ET in aqueous solutions, essentially all of the NMR studies were done in either pure organic solvents or organic solvent/water mixtures. But the solvents used varied from acetic acid to ethylene glycol or DMSO. It is not surprising, then, that the ET molecule, and especially its untethered tail, was seen to adopt different structures in these diverse environments. Because the various solvents result both in solutions with different pHs (causing different ionization states of the polar side chains) and have different hydrogen bonding potentials for interaction with the polypeptide backbone and side chains, it is reasonable to attribute some of the structural variations seen to environmental effects. However, not all the differences in structures can be accounted for in this manner because a number of the NMR studies were done in the same solvent but still produced different results. This could be a consequence of disparate data interpretation and peak assignment; the result of different calculation algorithms used and their manners of applying constraints; the product of the limited number of long-distance NOEs that are needed to define the tertiary structure; and/or the flexibility of the molecule, which could produce multiple conformers at equilibrium in solution, hence giving rise to averaged signals. Probably all of these other factors also contribute to the diversity of results obtained, suggesting all differences are not necessarily attributable only to real or environmental differences in the structures.

Given that so many different structures were produced by the single technique of NMR, it is not too surprising that signifi-
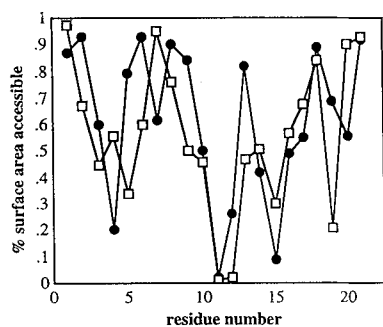

Fig. 5. Plot of surface accessibilities versus residue number for the X-ray (filled circles) and NMR (open squares) structures.
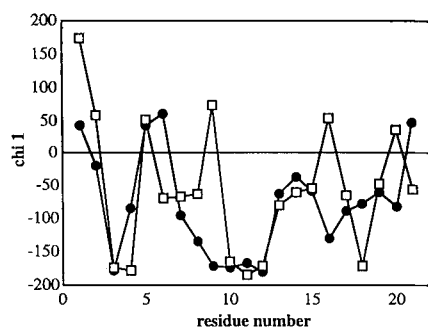

Fig. 6. Plot of chi1 angle versus residue number for the X-ray (filled circles) and NMR (open squares) structures.
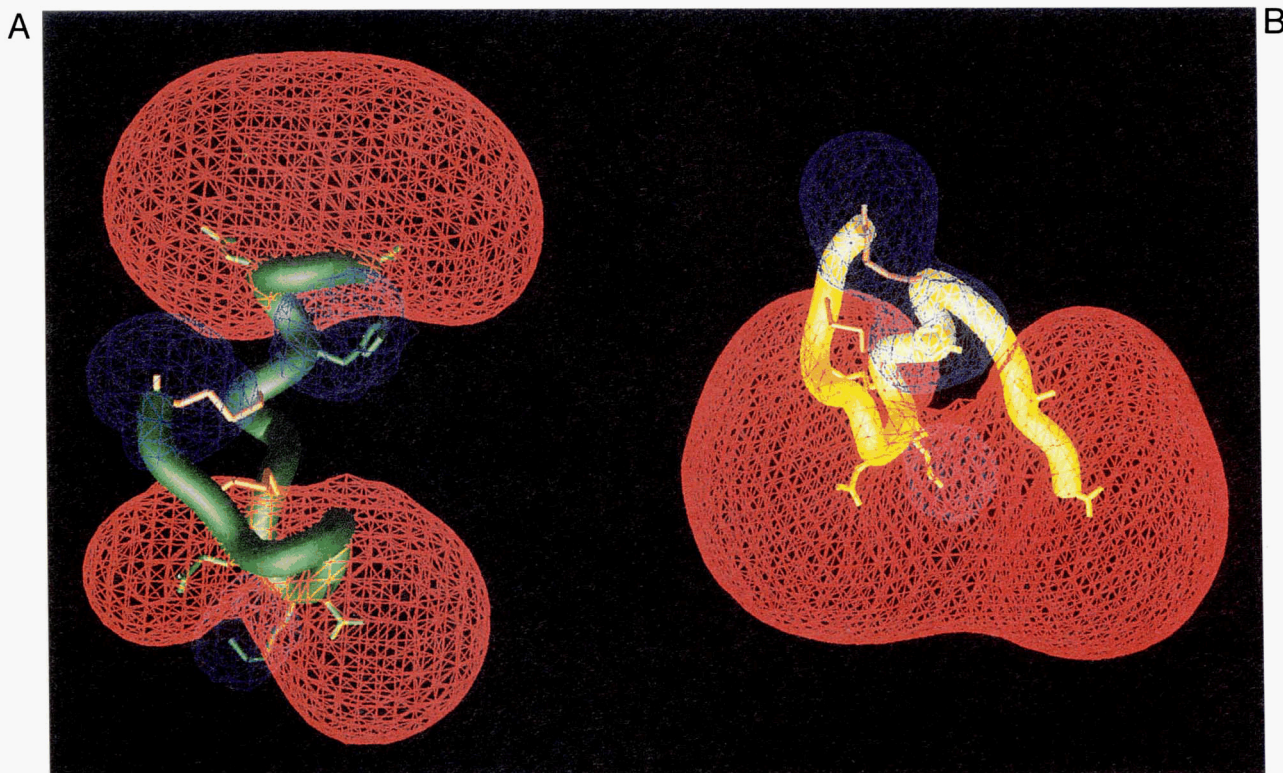
Fig. 7. GRASP plots showing the electrostatic potentials around the **(A)** X-ray and **(B)** NMR structures with the isopotential contours at +1 kT in blue and −1 kT in red.

cantly different models could arise from analyses by the two very different techniques of NMR and X-ray diffraction. One obvious consideration for the discrepancies is the chemical nature of the environment in the two experiments. The X-ray structure is from water, without any additives, whereas the closest NMR model that was used in our comparisons is from a solution of 60% ethylene glycol. Although the latter solvent does have hydrogen bonding characteristics similar to water, it is clearly different structurally, so some of the variation is likely due to the chemical environment. This is especially true in light of the variability with solvents seen among the NMR models described above. The next major consideration must be the physical nature of the environment: the NMR studies were done in isotropic solutions, where the polypeptide is in a monomeric state. The crystal studies were done in an anisotropic lattice, where crystal packing forces can potentially have major effects. This possibility has been carefully considered, especially with respect to

the packing of the C-terminus (Janes et al., 1994), and found not to be significant in the case of ET because none of the lattice contacts involve van der Waals interactions of the tails. In addition, the region around residue 9, which is the other major region of deviation, is also not involved in any intermolecular interactions in the crystal. Ironically, as stated previously, the region that does involve the most extensive crystal contact interactions is the region around residues 11–14, which is the part of the molecule most similar in the two structures. These results, then, tend to suggest that the physical environment is at most a minor factor in producing the different structures.

Table 2. *RMS deviations (in Å) from crystal structure (main-chain atoms only)*

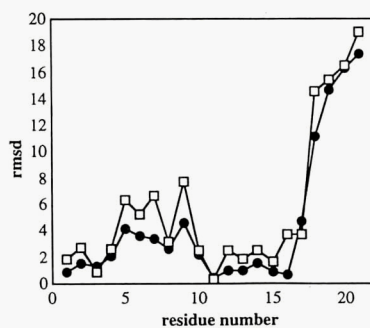| Model	Intact	1–15 only	S-S only
NMR-1	4.98	2.02	0.80
NMR-2	12.45	2.30	1.14
NMR-3	3.26	2.52	6.26
NMR-4	3.55	2.93	2.27

Fig. 8. Plot of the RMS deviations between the X-ray and NMR structures for each residue backbone atoms (filled circles) and side-chain atoms (open squares).
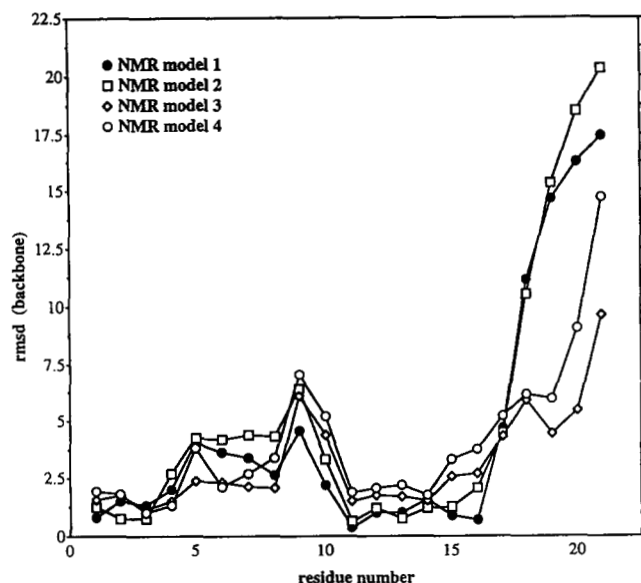
Fig. 9. Plot of RMS deviations versus residue number between the X-ray structure and all four NMR models described. Model 1 is shown in filled circles.

The most direct manner of determining whether the NMR data can be explained by the X-ray structure is to calculate the number of violations to the NOE constraint data that the X-ray structure would produce (Fig. 4B). There are only a few constraint violations for residues 1–8 and 16–21, suggesting that the NMR data are consistent with the conformation of the X-ray structure in these regions. But this may be misleading. The number of distance constraints (other than intraresidue or between adjacent residues) is very limited in the tail region (Fig. 4A), and this may be the reason for the lack of violations. The lack of long distance NOEs in the tail has been a common feature for all the NMR experiments reported to date. There are few violations of the constraints involving the cysteines, despite the fact that many of these are long-distance constraints, indicative of a consistent and well-defined disulfide region. The region of the X-ray structure from residue 9 to residue 14 produces most of the violations, and yet the backbone for this region is most similar to the backbone of the NMR model. That the X-ray structure appears to produce a relatively large number of NOE violations might be in part a result of the DISCON (Andersen et al., 1990) algorithm, which produces relatively narrow constraint boundaries. A seeming paradox is that Val 12 is the residue with the largest number of NOE violations (mostly involving its side-chain atoms) (Fig. 4B) whereas the NMR model has only a small RMS deviation from the X-ray structure in this region. This may in part be because Val 12 is the residue with the largest total number of constraints (other than the cysteines) (Fig. 4A), which gives it more potential for violations. Also, it is one of the regions of intermolecular contact in the crystal. Interestingly, the most frequent violations involving $C\alpha$ hydrogen atoms are those that have Lys 9 or Leu 6 as one member of the pair. Notably, these residues are the two Ramachandran outliers in the NMR structure, and thus a somewhat distorted NMR structure may have been produced in this region in order to accommodate the apparent measured NOEs.

Conformational flexibility may also contribute to differences seen between the X-ray and NMR structures. Although ET has two crosslinked disulfides, the NMR data of Krystek et al. (1991) and others (Table 1) support the idea that the N-terminal residues (1–3) and the C-terminal residues (16–21) show considerable conformational flexibility. Some local flexibility may well account for the differences in, say, Lys 9, the residue in the head that differs most between the structures. This residue has a higher than average temperature factor, suggesting flexibility in the X-ray structure, and is one of the Ramachandran outliers in the NMR structure, which may suggest that it arises from conformational averaging of two or more structures in this region. The NMR data suggest flexibility in the tail region. However, this is a well-ordered region in the crystal structure, so the X-ray data are not particularly supportive of tail flexibility. This means that as this is the region that is most sensitive to solvent effects, the different tail conformations in the X-ray and NMR structures are likely to be primarily reflecting a difference between aqueous and nonaqueous environments.

Of course, the principal question for all this work is: why are we concerned with details of the differences in the X-ray and NMR structures, especially if the overall folds are quite similar? The answer is that the very regions in which there are the biggest differences between the two structures (the loop between 6 and 9) and the tail are the regions that structure–activity relation studies have suggested are most critical for binding specificity and vasoactivity (Janes et al., 1994; Huggins et al., 1993) and so must be known precisely if they are to be of use in rational drug design studies. The loop region is where the greatest number of variable residues amongst the isoforms are located and has been implicated in the specificity of binding. Furthermore, a recent (Tam et al., 1994) alanine scan study of ET mutants speculated that their finding of the special sensitivity of residues 13, 14, 17, and 21 for ET binding and agonist activity would be most comprehensible if the entire C-terminus were helical in its biologically active form (thereby placing all these residues on the same surface), as it is in the X-ray structure. Thus, this comparative study was aimed at aiding the understanding of the underlying nature of the variation in the two structures, which may help to identify the most useful conformation for modeling of receptor/ligand interactions.

Discussion

In summary, these comparisons between the NMR and X-ray structures of human ET have provided us with the opportunity to examine the structural flexibility of this highly constrained intermediate-sized polypeptide and indicate significant differences between the structures as determined by the techniques of X-ray crystallography and NMR spectroscopy. They also provide information on the environmental factors that may account for some of the conformational differences reported between the structures in solution and in the crystalline state.

Methods

Models

The X-ray structure is that published in Janes et al. (1994). To summarize, the crystals were grown from pure aqueous solution at room temperature and had a solvent content of 36% solvent.

The structure was refined using RESTRAIN (Haneef et al., 1985) and XPLOR (Brünger, 1988). The RMS bond length deviation is 0.018 Å, with an $E(tot) = E(VDW) + E(ELEC) = -486$ kcal/mol (from XPLOR). According to PROCHECK (Laskowski et al., 1993), it has one Ramachandran outlier (Asp 8), and two chi1, chi2 outliers (His 16 and Asp 8). The coordinates have been deposited in the Brookhaven Protein Data Bank.

The NMR model is from Krystek et al. (1991). The solution studies were done at a concentration of 1.5–3.2 mM in 60% ethylene glycol at pH 3.2. Distance constraints were applied and refined using the DISCOVER protocol developed by Krystek et al. (1991). There were several ensembles of structures described in that work. In this paper, we designate the best model, the only one successful in producing the molecular replacement solution, as "model 1" or "the" NMR structure, the coordinates of which have been recently deposited in the Brookhaven Protein Data Bank. That structure was one of several ensembles of structures tested that was obtained directly from an NMR constraint set using 138 distance constraints incorporated in a distance-restrained molecular dynamics calculation. It has an RMS bond deviation of 0.015 Å, and an $E(tot) = -366$ kcal/mol (according to XPLOR). It has two Ramachandran outliers (Leu 6 and Lys 9), and two chi1, chi2 outliers (His 16 and Cys 11), which is not uncommon for structures of this size. Note that this is NOT the XPLOR-refined model from that same paper, the first 17 amino acid coordinates of which were deposited in the Brookhaven Protein Data Bank by N.H. Andersen and C. Chen as 1EDP. In that case, only one member of the ensemble, designated "the best-fitting single conformer" by the authors, was deposited. That model, which was not successful in producing a molecular replacement solution, we have designated as "model 3" in this work. Models 2 and 4 are alternative optimized models produced by the DISCOVER and XPLOR procedures, respectively, from the Krystek et al. (1991) paper.

Alignment

Because it was clear (from the molecular replacement studies and from visual inspection) that the C-terminal amino acids deviated significantly in position between the X-ray and NMR models, the first attempts at alignment were undertaken using only the backbone atoms from residues 1–15. The program MNYFIT (Sutcliffe et al., 1987) was used to define the regions with the highest correlations (residues 1–3 and 11–15). The alignment, based on the Cα atoms of these residues, was refined using XS6 (Šali & Blundell, 1990). Interestingly, very similar results were obtained if the alignment was done with only the four cysteine residues (all atoms), or with backbone atoms of all the residues from 1 to 15. Virtually identical results were obtained with the alternative algorithm BESTFIT (SERC Collaborative Computer Project No. 4, Daresbury Laboratory, UK) using the main-chain atoms of the residues from 1 to 15. Thus, the alignment was quite straightforward and relatively independent of the choice of atoms aligned or algorithm used. The overall RMS deviations reported are calculated with BESTFIT. The RMS deviations of individual residues and atoms in the aligned structures were calculated using XPLOR (Brünger, 1988).

Comparisons

Analyses were performed using the CCP4 suite of programs (SERC Collaborative Computer Project No. 4, Daresbury Laboratory, UK), including HBONDS, CONTACT, ANGLES, and AREA, as well as XPLOR (Brünger, 1988). Electrostatic calculations were performed using GRASP (Nicholls et al., 1993). The electrostatic potential was calculated at physiological ionic strength (0.15 M) (Sharp & Honig, 1990), using the full charge scheme to assign charges to the N- and C-termini and charged residues (Asp 8, Lys 9, Glu 10, His 16, and Asp 18). Graphical displays of the structures were produced using SETOR (Evans, 1993) and GRASP (Nicholls et al., 1993) software.

References

Andersen NH, Chen C, Marschner TM, Krystek SR Jr, Bassolino D. 1992. Conformational isomerism of endothelin in acidic aqueous media: A conformational NOESY analysis. *Biochemistry 31*:1280–1295.

Andersen NH, Lai X, Marschner T. 1990. *NOESYSIM/DISCON documentation.* Seattle: University of Washington.

Aumelas A, Chiche L, Mahe E, Le-Nguyen D, Sizun P, Berthault P, Perly B. 1991. Determination of the structure of (Nle[7])-endothelin by ^{1}H NMR. *Int J Pept Protein Res 37*:315–324.

Baldwin ET, Weber IT, St Charles R, Xuan JC, Appella E, Yamada M, Matsushima K, Edwards BFP, Clore GM, Gronenborn AM, Wlodawer A. 1991. Crystal structure of interleukin-8: Symbiosis of NMR and crystallography. *Proc Natl Acad Sci USA 88*:502–506.

Billeter M, Kline AD, Braun W, Huber R, Wüthrich K. 1989. Comparison of the high-resolution structures of the alpha-amylase inhibitor tendamistat determined by nuclear magnetic resonance in solution and by X-ray diffraction in single crystals. *J Mol Biol 206*:677–687.

Brünger AT. 1988. Crystallographic refinement by simulated annealing. Application to a 2.8-Å resolution structure of aspartate aminotransferase. *J Mol Biol 203*:803–816.

Brünger AT, Campbell RL, Clore GM, Gronenborn AM, Karplus M, Petsko GA, Teeter MM. 1987. Solution of a protein crystal structure with a model obtained from NMR interprotein distance restraints. *Science 235*:1049–1053.

Brünger AT, Clore GM, Gronenborn AM, Karplus M. 1986. Three-dimensional structure of proteins determined by molecular dynamics with interproton distance restraints: Application to crambin. *Proc Natl Acad Sci USA 83*:3801–3805.

Coles M, Munro SLA, Craik DJ. 1994. The solution structure of a monocyclic analog of endothelin [1,15 aba]-ET-1, determined by 1H-NMR spectroscopy. *J Med Chem 37*:656–664.

Dalgarno DC, Slater L, Chackalamannil S, Senior MM. 1992. Solution conformation of endothelin and point mutants by nuclear magnetic resonance spectroscopy. *Int J Pept Protein Res 40*:515–523.

Endo S, Inooka H, Ishibashi Y, Kitada C, Mizuta O, Fujino M. 1989. Solution conformation of endothelin determined by nuclear magnetic resonance and distance geometry. *FEBS Lett 257*:149–154.

Evans SV. 1993. SETOR — Hardware-lighted 3-dimensional solid model representations of macromolecules. *J Mol Graphics 11*:134.

Haneef I, Moss DS, Stanford MJ, Borkakoti N. 1985. Restrained structure-factor least-squares refinement using a vector processing computer. *Acta Crystallogr A 41*:426–433.

Huggins JP, Pelton JT, Miller RC. 1993. The structure and specificity of endothelin receptors: Their importance in physiology and medicine. *Pharmacol Ther 59*:55–123.

Janes RW, Peapus DH, Wallace BA. 1994. The crystal structure of human endothelin. *Nature Struct Biol 1*:311–319.

Janes RW, Wallace BA. 1994. Modelling the structure of the isoforms of human endothelin based on the crystal structure of human endothelin-1. *Biochem Trans 22*:1037–1042.

Krystek SR Jr, Bassolino DA, Novotny J, Chen C, Marschner TM, Andersen NH. 1991. Conformation of endothelin in aqueous ethylene glycol determined by ^{1}H-NMR and molecular dynamics simulations. *FEBS Lett 281*:212–218.

Laskowski RA, MacArthur MW, Moss DS, Thornton JM. 1993. PROCHECK — A program to check the stereochemical quality of protein structures. *J Appl Crystallogr 26*:283–291.

Lee B, Richards FM. 1971. The interpretation of protein structures: Estimation of static accessibility. *J Mol Biol 55*:379–400.

Munro S, Craik DJ, McConville D, Hall JG, Searle M, Bicknell W, Scanlon D, Chandler C. 1991. Solution conformation of endothelin, a potent vaso-constricting bicyclic peptide. A combined use of ^{1}H NMR and distance geometry calculations. *FEBS Lett 278*:9–13.

Nicholls A, Bharadwaj R, Honig B. 1993. GRASP—Graphical representation and analysis of surface-properties. *Biophys J 64*:166.

Reily MD, Dunbar JB Jr. 1991. The conformation of endothelin-1 in aqueous solution: NMR-derived constraints combined with distance geometry and molecular dynamics calculations. *Biochem Biophys Res Commun 178*:570–577.

Šali A, Blundell TL. 1990. Definition of general topological equivalence in protein structures—A procedure involving comparison of properties and relationships through simulated annealing and dynamic-programming. *J Mol Biol 212*:403–428.

Saudek V, Hoflack J, Pelton JT. 1989. ^{1}H-NMR study of endothelin, sequence-specific assignment of the spectrum and a solution structure. *FEBS Lett 257*:145–148.

Saudek V, Hoflack J, Pelton JT. 1991. Solution conformation of endothelin-1 by 1H-NMR, CD, and molecular modeling. *Int J Pept Protein Res 37*:174–179.

Shaanan B, Gronenborn AM, Cohen GH, Gilliland GL, Veerapandian B, Davies DR, Clore GM. 1992. Combining experimental information from crystal and solution studies. Joint X-ray and NMR refinement. *Science 257*:961–964.

Sharp K, Honig B. 1990. Calculating total electrostatic energies with the nonlinear Poisson–Boltzmann equation. *J Phys Chem 94*:7684–7692.

Smith LJ, Redfield C, Smith RAG, Dobson CM, Clore GM, Gronenborn AM, Walter MR, Naganbushan TL, Wlodawer A. 1994. Comparison of four independently determined structures of human recombinant interleukin-4. *Nature Struct Biol 1*:301–310.

Sutcliffe MJ, Haneef I, Carney D, Blundell TL. 1987. Knowledge based modeling of homologous proteins. 1. Three-dimensional frameworks derived for the simultaneous superposition of multiple structures. *Protein Eng 1*:377–384.

Tam JP, Liu W, Zhang JW, Galantino M, Bertolero F, Cristiani C, Vaghi F, DeCastiglione R. 1994. Alanine scan of endothelin: Importance of aromatic residues. *Peptides 15*:703–708.

Tamaoki H, Kobayashi Y, Nishimura S, Ohkubo T, Kyoguku Y, Nakajima K, Kumagaye S, Kimura T, Sakakibara S. 1991. Solution conformation of endothelin determined by means of ^{1}H NMR spectroscopy and distance geometry calculations. *Protein Eng 4*:509–518.